Supporting Information

Photodynamic Hydrogen-Bonded Biohybrid Framework: A Photo-Bio-Catalytic Cascade Nanoreactor for Accelerating Diabetic Wound Therapy

Wei Huang[a†], Haitao Yuan[c†], Huangsheng Yang[b], Linjing Tong[b], Rui Gao[b], Xiaoxue Kou[b], Jigang Wang[c]*, Xiaomin Ma[e], Siming Huang[d]*, Fang Zhu[b], Guosheng Chen[b]* and Gangfeng Ouyang[a,b]

[a]School of Chemical Engineering and Technology, Sun Yat-sen University, Zhuhai 519082, China

[b]MOE Key Laboratory of Bioinorganic and Synthetic Chemistry, School of Chemistry, Sun Yat-sen University, Guangzhou 510275, China

[c]Department of Geriatric Medicine, Shenzhen People's Hospital (The Second Clinical Medical College, Jinan University), Shenzhen 518020, China.

[d]Guangzhou Municipal and Guangdong Provincial Key Laboratory of Molecular Target & Clinical Pharmacology, the NMPA and State Key Laboratory of Respiratory Disease, School of Pharmaceutical Sciences and the Fifth Affiliated Hospital, Guangzhou Medical University, Guangzhou 511436, China

[e]Cryo-EM Center, Southern University of Science and Technology, Shenzhen 518055, China

[†]These authors contributed equally

*Email: jgwang@icmm.ac.cn; huangsm@gzhmu.edu.cn; chengsh39@mail.sysu.edu.cn;

1. Supplementary Methods

1.1. Reagents and materials.

Enzymes including glucose oxidase (GOx), catalase (CAT), horseradish peroxidase (HRP), and other reagents including glucose and 3,3',5,5'-tetramethylbenzidine (TMB) were obtained from Aladdin Chemistry Co., Ltd. (Shanghai, China). 1,3,6,8-tetrakis (p-benzoic acid) pyrene (H4TBAPy), 2-methylimidazole (HmIM) and zinc acetate dihydrate were purchased from J&K Scientific (Beijing, China). Polyvinylpyrrolidone (PVP), Chlorin e6 (Ce6), fluorescein isothiocyanate (FITC) and Rhodamine B isothiocyanate (RhB) were purchased from Macklin Biochemical Technology Co., Ltd. (Shanghai, China). Dimethyl formamide (DMF) and ethanol were purchased from Guangzhou Chemical Reagent Factory (Guangzhou, China). SYTO 9 and Propidium iodide (PI) were purchased from Thermo Fisher Scientific, Inc. All chemicals and reagents were purchased from commercial sources and used without further purification.

1.2. Characterization.

Powder X-ray diffraction (PXRD) patterns were collected (0.02°/step, 0.06 seconds/step) on a Bruker D8 Advance diffractometer (Cu Kα) at room temperature.

N_2 adsorption/desorption isotherms were collected with a JW-DX Surface Area Analyzer at -196 °C. All the samples were pre-treated under 100 °C for 12 h before measurements.

The ultraviolet-visible (UV-Vis) absorbance measurement was carried out on a 2800S spectrophotometer (SOPTOP, Shanghai).

Fourier transform infrared (FTIR) spectroscopy was performed with a Bruker EQUINOX 55 spectrometer (32 scans in the 4000-400 cm^{-1} spectral range).

The morphology images of the crystals were taken on a SU8010 ultra-high resolution field emission scanning electron microscope (SEM, Hitachi, Japan).

Confocal laser scanning microscope (CLSM 880 NLO, Carl Zeiss, Göttingen, Germany) was used to determine the distribution of dye-labelled enzymes within HOF-101 and ZIF-8.

Cryo-EM were performed on a FEI Titan Krios G3i (D3845) TEM operated at 300 kV and equipped with an autoloading mechanism, and the images were taken at a nominal magnification of 350,000 with a pixel size of 0.34 Å by 0.34 Å.

Zeta potentials were measured on a Nano ZS 90 system.

Fluorescence spectra were performed on an F-97 Pro fluorescence spectrometer.

Electron paramagnetic resonance (EPR, A300, Bruker Co., Germany) was utilized for the detection of radical generation.

1.3. Cryo-EM data acquisition.

Cryo-EM experiments were carried out according to our previous work.[1] All cryo-EM experiments were performed on a ThermoFisher Scientific Titan Krios G3i electron microscopes operated at 300 kV. The dispersive nanomaterials (in ethanol) were mounted to a carbon-coated TEM-grid and dried under vacuum. The specimen was

then dropped into liquid nitrogen and transferred by a Cryo-transfer loader into the microscope. Cryo-EM images were collected by a K3 Summit direct electron detector equipped with a GIF Quantum energy filter (slit width 20 eV) in the counting mode (Bin 0.5). Data acquisition was performed using SerialEM 3.864 with a nominal magnification of 350,000 ×, corresponding to a physical pixel size of 0.34 Å. The dose rate was ~15 counts/pixel/second, and the exposure time in a frame was 0.023 s. Each micrograph stack contains 10 frames (the total exposure time was 0.23 s), and the total dose rate was ca. 30 $e^-/Å^2$ per micrograph. The motion correction was performed using MotionCorr265 with 2×2 binning, and the non-dose-weighted sum of all frames from each movie was used for all image processing steps. The lattice spacing of HBFs unit cells were analyzed using DigitalMicrograph (Gatan) software.

1.4. Optimization of the GOx: CAT ratio in the assembly

The ratio of GOx to CAT during the preparation of Ce6@EnHOF-101 was optimized. According to the synthesis procedures mentioned in Ce6@EnHOF-101, 9 mL, pH=4 enzymes solution containing 2.5 mg GOx and 2.5 mg CAT was replaced by 9 mL, pH=4 enzymes solutions containing 2.5 mg GOx and 2.5 mg CAT (GOx: CAT = 1: 1), 2.5 mg GOx and 5.0 mg CAT (GOx: CAT = 1: 2), 2.5 mg GOx and 10.0 mg CAT (GOx: CAT = 1: 4), 5.0 mg GOx and 2.5 mg CAT (GOx: CAT = 2: 1), and 10.0 mg GOx and 2.5 mg CAT (GOx: CAT = 4: 1), respectively. In addition, the Ce6 loading step was removed, while other steps were consistent with that of Ce6@EnHOF-101 (seen in Methods section in main text).

1.5. Synthesis of GHHOF-101.

For the synthesis of GHHOF-101, 9 mL pH=4 enzymes solution containing 2.5 mg GOx and 2.5 mg CAT was replaced by 9 mL pH=4 enzymes aqueous solution containing 2.5 mg GOx and 2.5 mg HRP, and the Ce6 loading step was removed, while other steps were consistent with the synthesis procedures of Ce6@EnHOF-101.

1.6. Synthesis of GHOF-101.

For the synthesis of GHOF-101 hybrid, 9 mL, pH=4 enzymes solution containing 2.5 mg GOx and 2.5 mg CAT was replaced by 9 mL, pH=4 enzymes solution containing 2.5 mg GOx, and the Ce6 loading step was removed, while other steps were consistent with the synthesis procedures of Ce6@EnHOF-101.

1.7. Synthesis of CHOF-101 hybrid.

For the synthesis of CHOF-101 hybrid, 9 mL, pH=4 multienzymes (2.5 mg GOx and 2.5 mg CAT) mixed aqueous solution was replaced by 9 mL, CAT (2.5 mg) aqueous solution, and the Ce6 loading step was removed, while other steps were consistent with the synthesis procedures of Ce6@EnHOF-101.

1.8. Synthesis of EnHOF hybrid.

For the synthesis of EnHOF-101 hybrid, the Ce6 loading step was removed, while other steps are consistent with the synthesis procedures of Ce6@EnHOF-101.

1.9. Synthesis of Ce6@HOF-101 hybrid.

For the synthesis of Ce6@HOF-101 hybrid, 9 mL, pH=4 enzymes aqueous solution was replaced by 9 mL, pH=4 aqueous solution, while other steps are consistent with the synthesis procedures of Ce6@EnHOF-101.

1.10. Synthesis of Ce6@EnZIF-8.

Considering the microporous structure of ZIF-8 (ca. 3.4 Å aperture, Figure S13), the relatively large Ce6 (ca. 16.1×14.0 Å, Figure S6) was impossible to be loaded into the pore of ZIF-8 by the post-infiltration method. Thus, the Ce6@EnZIF-8 was synthesized via a "one-pot" assembling method.[2,3] In a typical process, a certain amount of enzymes powders (1 mg GOx and 1 mg CAT) were dispersed into 2 mL HmIM solution (1.2 M) through ultrasonic treatment, and this solution was termed as solution **A**. Then, 133 μL Ce6 (10 mg/mL in DMF) was added into 2 mL zinc acetate solution (0.1 M), and this solution was termed as solution **B**. Subsequently, the solution **B** was quickly poured into the solution A, and aged for 4 h at room temperature in the dark. After centrifugation, the obtained Ce6@EnZIF-8 precipitate was dispersed in 5 mL PVP aqueous solution (4 mg/mL), and stirred at room temperature for 2 h in dark condition. Finally, the prepared Ce6@EnZIF-8 precipitate was collected by centrifugation, washed by deionized water three times.

1.11. Preparation of standard HOF-101

The standard HOF-101 was prepared according to the reported method.[4] 150 mg H4TBAPy (0.225 mM) was dissolved in 22.5 mL of DMF to which 90 mL MeOH was added. The mixed solution was stirred for 1 min, and stood at room temperature for 12 h to afford the standard crystals of HOF-101. Finally, the product was collected by centrifugation, washed by ethanol three times and dried under vacuum at room temperature.

1.12. Fluorescence labeling of enzymes.

The fluorescence labeling experiment were carried out based on the conjugation between the amino of lysine residue of enzymes and the thiocarbmide of fluorescence dyes. In brief, 10 mg enzyme was dispersed into 1 mL carbonate buffer solution (pH=9.0, 0.5 M), followed by adding 1 mg fluorescence dyes (FITC or RhB). The mixed solution was then stirred for 12 h in dark condition. Finally, the FITC- or RhB-labelled enzymes were obtained through ultrafiltration by a centrifugal filter device (molecular weight cut-off MWCO= 8 kDa) for 3 times to remove excess reaction reagents and salts.

1.13. CLSM experiment

For the CLSM experiment, the GOx was labelled by RhB (denoted as RhB-GOx), while the CAT was labelled by FITC (denoted as FITC-CAT). The raw GOx and CAT was replaced by RhB-GOx and FITC-CAT to prepare the EnHOF-101 and EnZIF-8 as described above. Since the strong fluorescence interference of Ce6, the Ce6 loading

step was removed for clarifying the spatial distributions of RhB-GOx (red fluorescence, excitation wavelength: 552 nm) and FITC-CAT (green fluorescence, excitation wavelength: 488 nm). Noted that the HOF-101 has weak green fluorescence, which has been deducted in the CLSM imaging of FITC-CAT.

1.14. The enzymes adsorption experiment.

The enzymes adsorption experiment by as-synthesized standard HOF-101 was used to demonstrate the successful encapsulation of enzymes. In briefly, 2.5 mg GOx and 2.5 mg CAT were dispersed in 10 mL as-synthesized standard HOF-101 solution (1mg/mL). The mixed solution was stirred at room temperature for 5 min, and aged for another 15 min. Then, the free enzymes in the supernatant were collected by centrifugation, and quantified by a Bradford proteins assay.[5] The possibility of the surface-adsorption of enzymes onto or the post-infiltration of enzymes into HOF-101 was evaluated by examining the concentration differences of enzymes in the supernatant before and after adsorption.

1.15. Single enzyme loading measurement in GHOF-101 and CHOF-101

The loading efficiencies of GOx (in GHOF-101) and CAT (in CHOF-101) were measured by examining the concentration differences of proteins in the supernatant before and after encapsulation *via* a standard Bradford proteins assay.[5] Typically, 20 μL enzyme sample was added into a 96-well plate, followed by introducing 200 μL Coomassie Brilliant Blue G-250 reagent. After 5 min incubation, the solution was collected and detected by UV-Vis spectrophotometer. The concentration of the enzyme was proportional to the absorption strength at 595 nm, and was quantified using a calibration curve.

1.16. The activity of glucose decomposition

The activity of glucose decomposition of EnHOF-101 was evaluated based on the time-dependent glucose and pH change (equation 1). 1 mg/mL EnHOF-101 catalyst was used, and 20 mM glucose was added to activate the biocatalysis in the opening environment.

$$\text{glucose} + O_2 \xrightarrow{GOx} \text{gluconic acid} + H_2O_2 \qquad (1)$$

The time-dependent pH in the supernatant, attributing to the generated gluconic acid, was monitored using a pH meter.

The time-dependent glucose concentration in the supernatant was measured by an enzymatic assay. Briefly, the collected supernatant after reaction for a certain interval was incubated in a solution containing 0.625 μg/mL GOx, 0.625 μg/mL HRP and 300 μM TMB. After 2 min, the solution was collected was carefully collected by a pipette, and the glucose concentration was proportional to the UV Abs at 652 nm

For evaluating the activities of glucose decomposition of EnZIF-8 and GHOF-101, the EnHOF-101 was replaced by the equal quality of EnZIF-8 or GHOF-101 sample, while other steps were kept the same.

1.17. The activity of O_2 generation

CAT could catalyze H_2O_2 into O_2 (equation 2):

$$H_2O_2 \xrightarrow{CAT} H_2O + O_2 \qquad (2)$$

The time-dependent O_2 generation was evaluated by a portable dissolved oxygen meter, wherein EnHOF-101 (1 mg/mL) was dispersed into 5 mL aqueous solution, 5 mL 20 mM glucose solution or 5 mL 20 mM H_2O_2 solution, respectively.

As a comparison, the activity of O_2 generation of EnZIF-8 was also examined using the similar method.

1.18. Reactive oxygen species (ROS) measurement by fluorescence spectroscopy

Activated 2', 7'-dichlorofluorescin (DCFH) was prepared according to the procedure in the literature.[6] Briefly, 10 μL sample solution was added into 1 mL activated DCFH (40 μM), respectively. Then, the mixed solution was undergone the white light irradiation (45 mW/cm^2) for 3 min. Finally, the emission spectra were monitored by fluorescence measurements and recorded at 525 nm with the excitation wavelength of 488 nm. The intensity of fluorescence at 525 nm was proportional to the ROS amounts.

1.19. Time-dependent bacteria-growth experiment

The bacteria-growth experiments were divided into 8 groups: (1) PBS, (2) HOF-101, (3) Ce6@HOF-101, (4) Ce6@EnHOF-101, (5) PBS+light, (6) HOF-101+light, (7) Ce6@HOF-101+light, (8) Ce6@EnHOF-101+light. The concentrations of different nanoparticles, sterile PBS, and glucose used in the experiment were 500 μg/mL, 10 mM, and 20 mM, respectively. Firstly, MRSA solutions (OD_{600} = 1.0) were mixed with the sample solutions of groups (1) to (8), respectively, and incubated for 30 min at 37 ^oC. Then, the pathogens suspension was diluted 10 fold with sterile PBS and, next, 100 μL diluted pathogens suspension was added into a 96-well plate. Then, the groups (5) to (8) were undergone a white light irradiation (45 mW/cm^2) for 10 min, while the group (1) to (4) were stood in the dark for 10 min. Finally, all of the 96-well plates were incubated in an incubator at 37 ^oC for 4h, 8h and 12, respectively. The bacteria-growth in each group was evaluated based on the change of OD_{600} value.

1.20. The live/dead assay to examine bacterial viability

After treatments in different groups, the pathogens were washed with sterile PBS, and collected by centrifugation at 7300 rpm for 3 min. The collected pathogens were resuspended into 100 μL sterile PBS, and were stained by the mixture of SYTO 9 (50 μL, 0.2 mM) and propidium iodide (PI) (50 μL, 0.2 mM) fluorescent dyes in the dark at 37 ^oC for 0.5 h. After washing with sterile PBS, the samples (10 μL) were dropped onto the slide for fixation. The fluorescence imaging of *MRSA* was performed by laser scanning confocal microscope (TCS SP8, Leica, Germany).

1.21. SEM characterization for bacterial samples

After treatments in different groups, the pathogens were washed with sterile PBS, and collected by centrifugation at 7300 rpm for 3 min. The collected pathogens were resuspended into 100 μL sterile PBS. Then, 2-3 μL pathogens suspension was dropped onto the clean silicon slice, and dried in air naturally. After that, 2.5% glutaraldehyde solution was added to fix the pathogens overnight. Next, the bacterial cells were washed with sterile PBS, and then dehydrated using various concentrations of ethanol solutions (10%, 30%, 50%, 70%, 80% and 100%). Finally, the dehydrated bacteria cells were sputter-coated with Au for SEM imaging.

1.22. Hemolysis assay

Briefly, 1 mL of 4% erythrocytes (v/v) was mixed with various concentrations (0, 250, 500, 1000 and 2000 μg/mL) of Ce6@EnHOF-101 and 2% triton × 100. After incubated at 37 °C for 4 h, the mixture was centrifuged and the supernatant was collected. Then, the absorbance of the supernatant at 542 nm was measured by a microplate reader. The percentage of hemolysis was calculated using the following equation (3)[7]:

$$\text{Hemolysis (\%)} = (I/I_0) \times 100\% \qquad (3)$$

Where I refers to the optical density (OD) of erythrocytes after the incubation with different concentrations of Ce6@EnHOF-101, and I_0 means the optical density (OD) of the complete hemolysis in PBS.

1.23. Cytotoxicity assay

The 293T normal cells were inoculated in a 96-well plate with a density of 5×10^3 cells per well, respectively. The cells were cultured for 24 h, and then the Ce6@EnHOF-101 solutions with different concentrations were added, respectively. After incubation for another 12 h, the medium was discarded, followed by the addition of 100 μL, 1 mg/mL thiazolyl tetrazolium (MTT) into each wells, and then cultured at 37 °C for 4 h. Subsequently, the supernatant was discarded, and 100 μL DMSO solution was added into each well. The final samples were analyzed by a microplate reader. The absorbance value at 520 nm was determined, and used to evaluate the cell viability according to the following equation (4):

$$\text{Cell viability} = A/A_0 \times 100\% \qquad (4)$$

Where A is the absorbance value of the experimental group, and A_0 is the absorbance value of the blank group without any treatment.

Supplementary tables

Table S1. The enzymes dosage used and the loading efficiency in the biocascade nanoreactor with bi-enzymes.

biocascade nanoreactor	enzymes	dosage[a] (mg/mL)	loading[b] (w/w%)
EnHOF-101	CAT	0.25	18.3
	GOx	0.25	15.8
EnZIF-8	CAT	0.25	1.8
	GOx	0.25	2.5

a.The dosage (mg/mL) means the enzymes concentration in the initial assembly system.

b.The loading (w/w) of each enzymes was calculated based on the assembly experiment using fluorescence labelled enzymes.

Table S2. The enzymes dosage used and the loading efficiency in the nanoreactor with single enzyme.

nanoreactor	dosage[a] (mg/mL)	loading[b] (w/w%)
GHOF-101	0.25	24.6
CHOF-101	0.25	24.1

a.The dosage (mg/mL) means the enzymes concentration in the initial assembly system.

b.The loading (w/w) of each enzymes was calculated based on the standard Bradford assay.

Table S3. The Ce6 dosage used and the calculated loading in different biocascade nanoreactor.

Sample	dosage[a] (mg/mL)	loading[b] (w/w%)
Ce6@EnHOF-101	0.20	23.9
Ce6@EnZIF-8	0.33	4.3

a.The dosage (mg/mL) means the Ce6 concentration in the initial assembly system.

b.The loading (w/w) of Ce6 was quantified by UV-Vis spectroscopy according to the standard curve (Figure S14).

Supplementary Figures

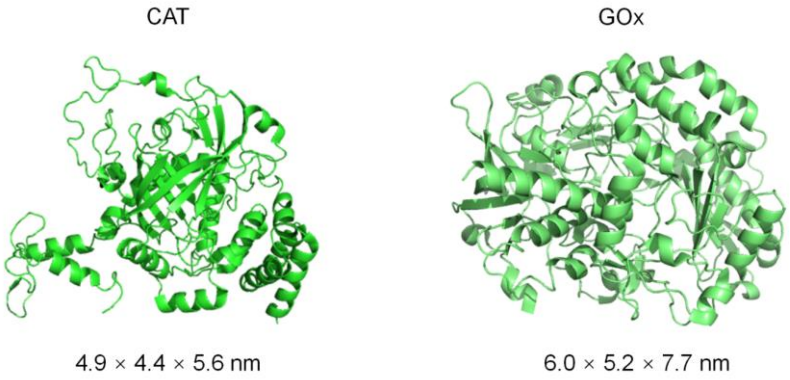

Figure S1. The molecular dimensions of CAT and GOx based on the PyMOL Molecular Graphics System (Version 2.4.0).

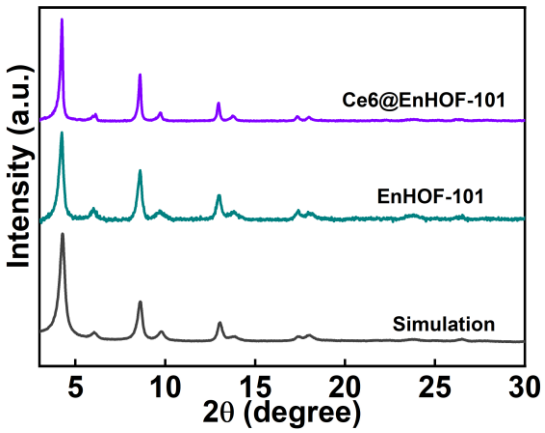

Figure S2. PXRD patterns of synthesized EnHOF-101 and Ce6@EnHOF-101.

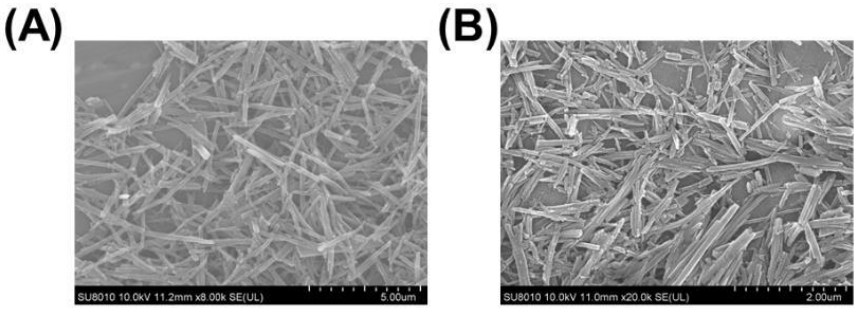

Figure S3. SEM images of (A) Ce6@EnHOF-101 and (B) pure HOF-101. Both Ce6@EnHOF-101 and pure HOF-101 showed the rod-like nanostructure.

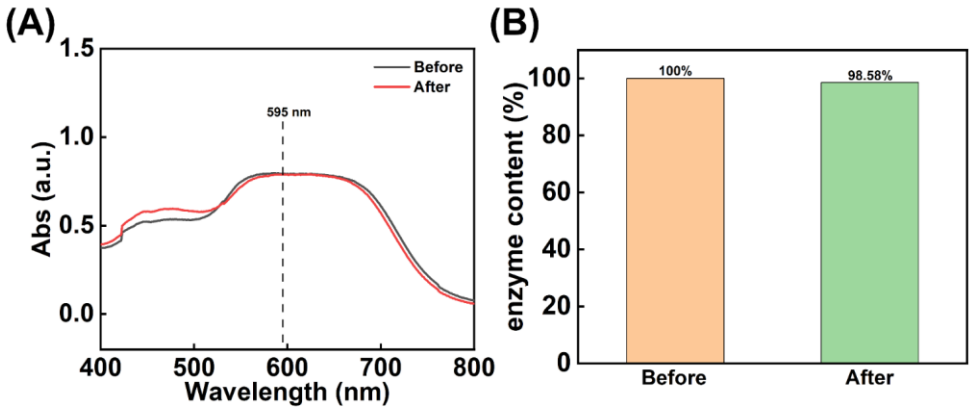

Figure S4. (A) The UV spectra of the supernatants before and after adsorption experiment. (B) The calculated enzyme contents in the supernatants before and after adsorption experiment. The enzyme concentration was proportional to the UV-Vis adsorption intensity at 595 nm.

The relative narrow mesopore in HOF-101 (ca. 2.0 nm, Figure 1D) was not insufficient to accommodate the bulky GOx and CAT (the molecular dimensions of GOx are ca. 6.0 nm × 5.2 nm × 7.7 nm, and CAT are ca. 4.9 nm × 4.4 nm × 5.6 nm, Figure S1). Given this, 2.5 mg GOx and 2.5 mg CAT were dispersed in 10 mL as-synthesized HOF-101solution (1 mg/mL). After 5 min stirring and 15 min standing, the GOx and CAT-adsorbed HOF-101 was collected, and the surface-adsorbed enzymes by HOF-101 were evaluated based on the concentration change of the enzymes in the supernatants before and after adsorption using standard Bradford assays. The UV spectra of the collected supernatants showed that almost no enzyme was surface-adsorbed by HOF-101 (Figure S4).

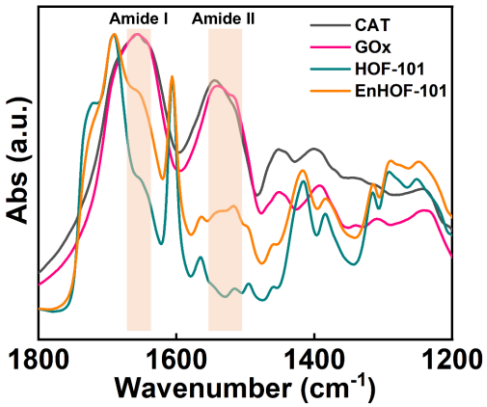

Figure S5. FTIR spectra of CAT, GOx, HOF-101 and EnHOF-101.

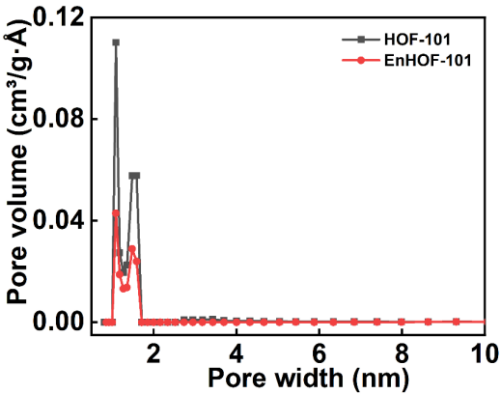

Figure S6. The pore-size distributions of HOF-101 and EnHOF-101.

Compared to HOF-101, EnHOF-101 showed a deceased pore volume. This was caused by the spatial occupation by the enzymes, which further demonstrated that the enzymes were indeed encapsulated into, rather than surface-adsorbed onto the HOF-101.

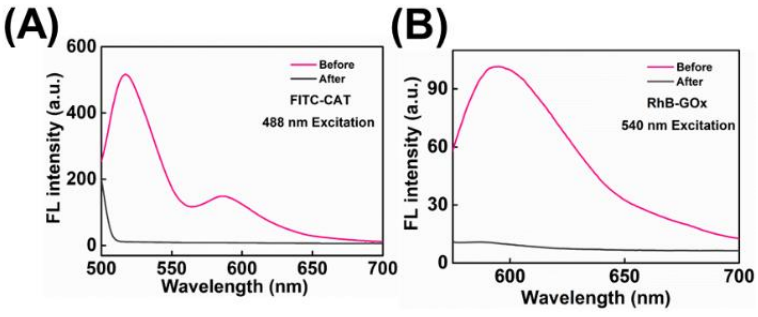

Figure S7. The fluorescent spectra of FITC-CAT and RhB-GOx in the supernatants before (A) and after (B) encapsulation by HOF-101.

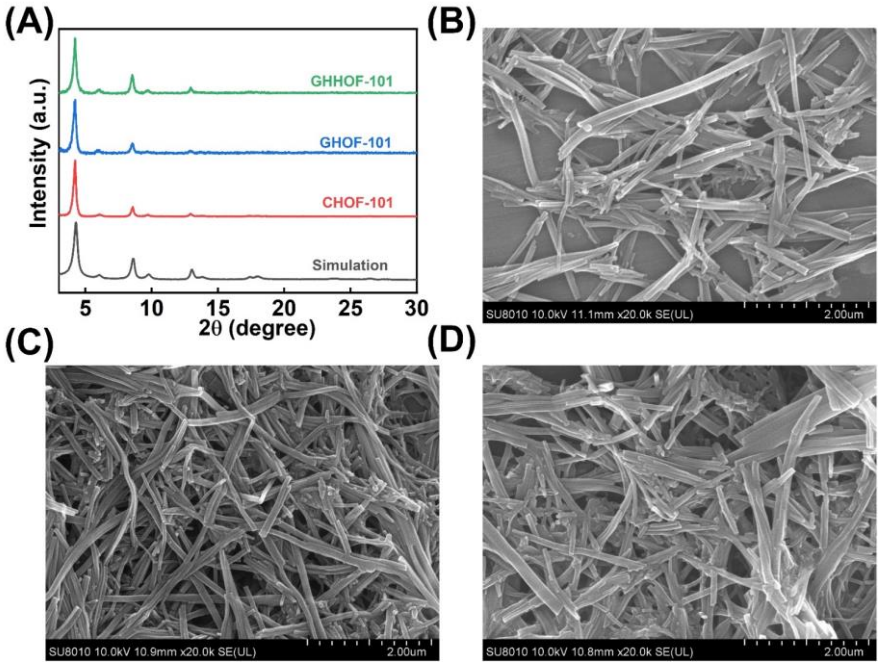

Figure S8. (A) PXRD patterns of prepared materials. The SEM images of GHOF-101 (B), CHOF-101 (C) and GHHOF-101 (D), respectively.

The PXRD patterns of the as-synthesized GHHOF-101, GHOF-101 and CHOF-101 well inherited the Bragg diffraction peaks of parent HOF-101, indicating that the crystallinity of these frameworks was reserved. The SEM images presented the rod-like nanostructure of the as-synthesized GHHOF-101, GHOF-101 and CHOF-101, which were in agreement with that of HOF-101 (Figure S3B). Both PXRD patterns and SEM images demonstrated the successful preparation of GHHOF-101, GHOF-101 and CHOF-101.

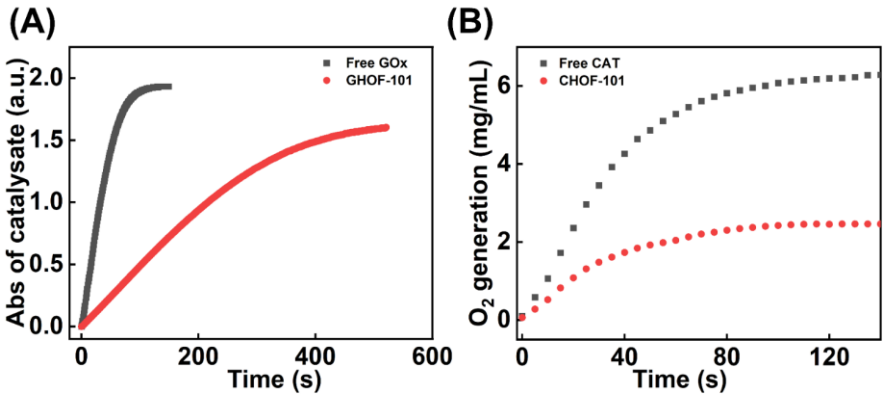

Figure S9. (A) The catalytic kinetics of free GOx and GHOF-101. The dosages of GOx was kept at 25 μg/mL in both groups; glucose was 2.17 mM. (B) The catalytic kinetics of free CAT and CHOF-101. The dosages of CAT was kept at 10 μg/mL in both groups; H_2O_2 was 2 mM.

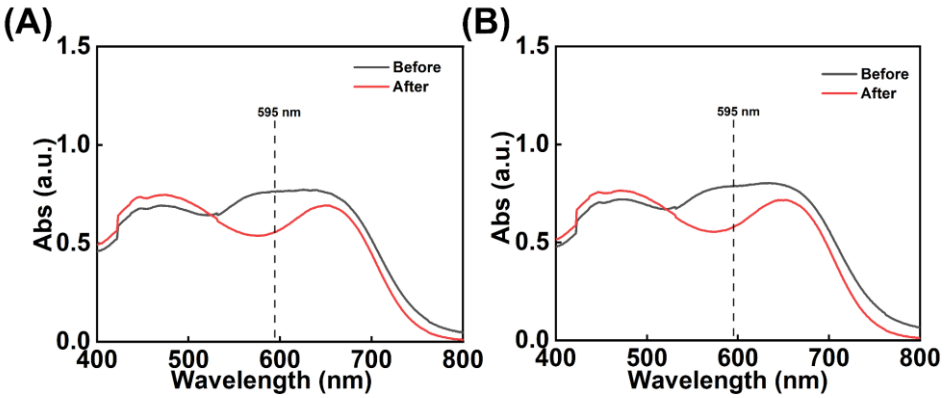

Figure S10. The standard Bradford protein assay of the collected supernatants before and after encapsulation of GOx (A) or CAT (B) by HOF-101, respectively. The enzyme concentration in the supernatants was proportional to the UV-Vis adsorption intensity at 595 nm.

The enzyme loading efficiencies, calculated according to concentration changes of enzymes in the supernatants before and after encapsulation by standard Bradford protein assays, were ca. 24.6 wt% and 24.1 wt% for CAT and GOx, respectively (Table S2).

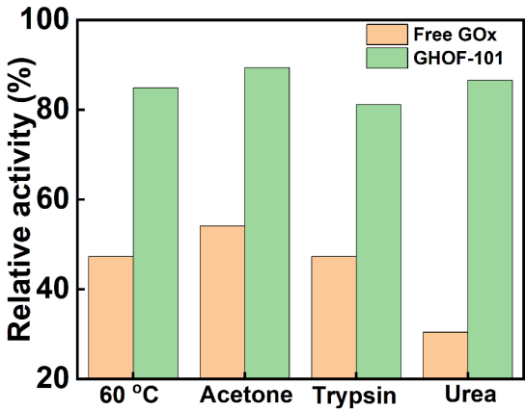

Figure S11. The retained bioactivity of GHOF-101 and free GOx after different treatments for 30 min.

Enzymes are susceptible to the external stimuli, which significantly hindered the enzymes for large-scale applications. Thus, the structural stability of the enzyme is of vital importance for industrial applications. In our work, the robust and porous HOF-101 “coating” could shield the guest enzymes against denaturation. In Figure S11, compared with the free GOx, higher activity conversions were observed in GHOF-101 after the treatments by high temperature (60 °C), denatured reagent (6 M urea), proteolytic enzyme (5 mg/mL trypsin), and polar solvent (acetone), respectively. It suggested that the HOF shell could improve the durability of the fragile enzymes.

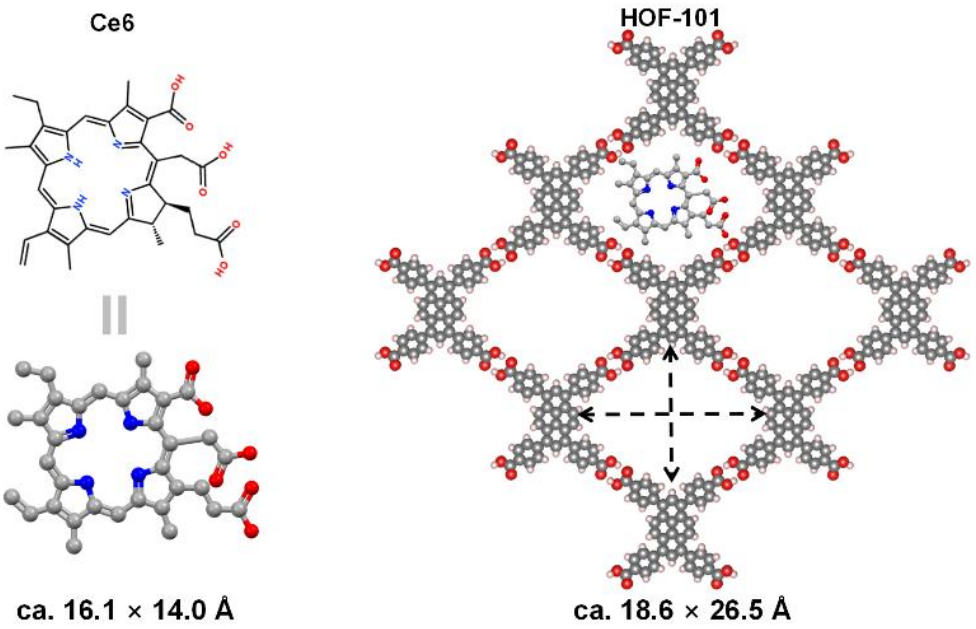

Figure S12. The chemical structures of Ce6 and the mesopore structure of HOF-101.

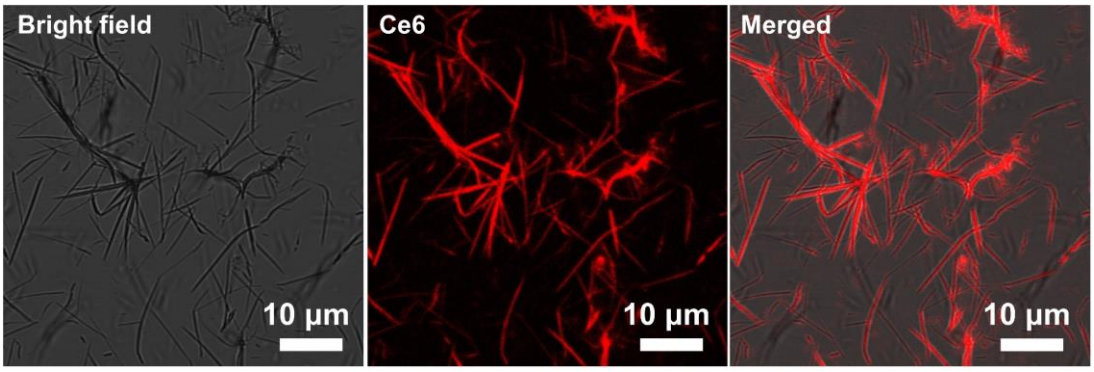

Figure S13. CLSM imaging of EnHOF-101 after the permeability of Ce6 into its cavity. Excitation wavelength: 405 nm.

Ce6 has a strong red fluorescence under excitation at 405 nm. To prove the permeability of Ce6 into HOF-101, we have carried out another confocal laser scanning microscope (CLSM) experiment. The Ce6 was dispersed in the as-synthesized EnHOF-101 solution and stirred for 10 min, then the Ce6-adsorbed EnHOF-101 was collected for CLSM imaging. As shown in Figure S13, the overlapped red fluorescence elucidated that the Ce6 was uniformly distributed within the whole HOF-101. This result indicated that the Ce6 was indeed anchored inside the HOFs, rather than adsorbed on the outer surface.

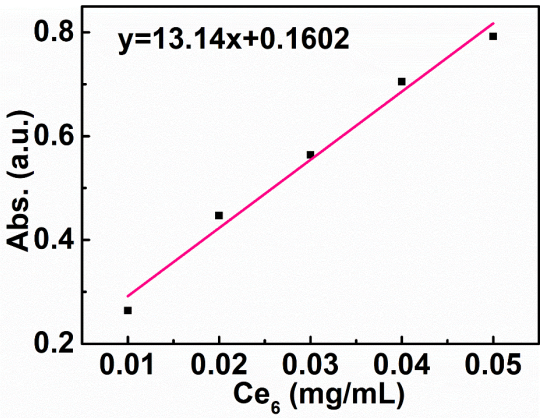

Figure S14. The standard curve for Ce6 quantification *via* UV–vis spectroscopy.

The loading efficiency of EnHOF-101 for Ce6 has been quantified by UV-Vis spectroscopy according to the standard curve (Figure S14), and the calculated loading was ca. 23.9% (w/w) and 4.3% (w/w) for Ce6@EnHOF-101 and Ce6@EnZIF-8, respectively. The high loading efficiency in Ce6@EnHOF-101 indicated that the well-arranged mesochannel favored the Ce6 loading.

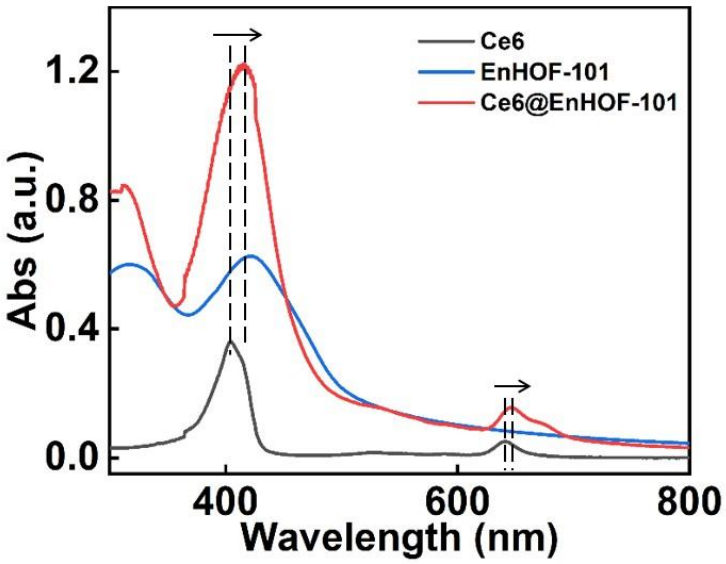

Figure S15. UV-Vis spectra of free Ce6, EnHOF-101 and Ce6@EnHOF-101.

We provided the UV-Vis absorption spectra of Ce6, EnHOF-101 and Ce6@EnHOF-101 in Figure S15. Compared with EnHOF-101, the typical UV-Vis absorption spectrum of Ce6 emerged in the resultant Ce6@EnHOF-101, suggesting that the Ce6 was successfully loaded into the mesochannels of HOF-101. In addition, we found that the absorption bands of Ce6 were slightly red-shifted after loading, indicating the host-guest interaction between Ce6 and HOF-101 scaffold.

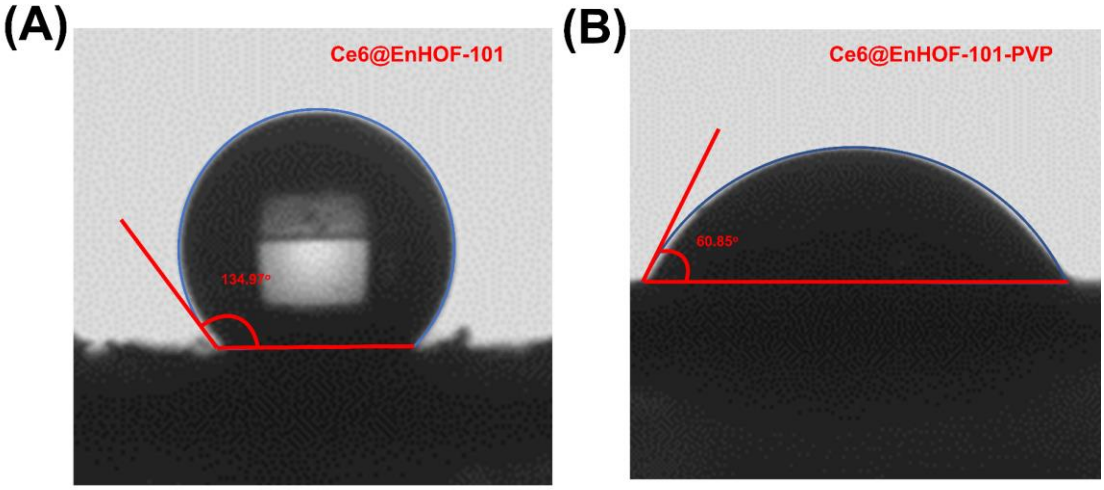

Figure S16. The contact angle test of (A) the raw Ce6@EnHOF-101 and (B) the Ce6@EnHOF-101 modified with PVP (Ce6@EnHOF-101-PVP).

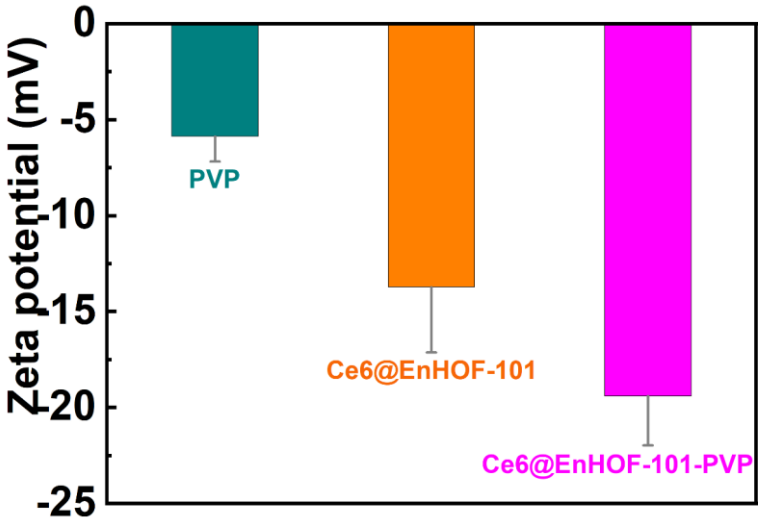

Figure S17. The Zeta potentials of PVP, Ce6@EnHOF-101 and Ce6@EnHOF-101 modified with PVP (Ce6@EnHOF-101-PVP).

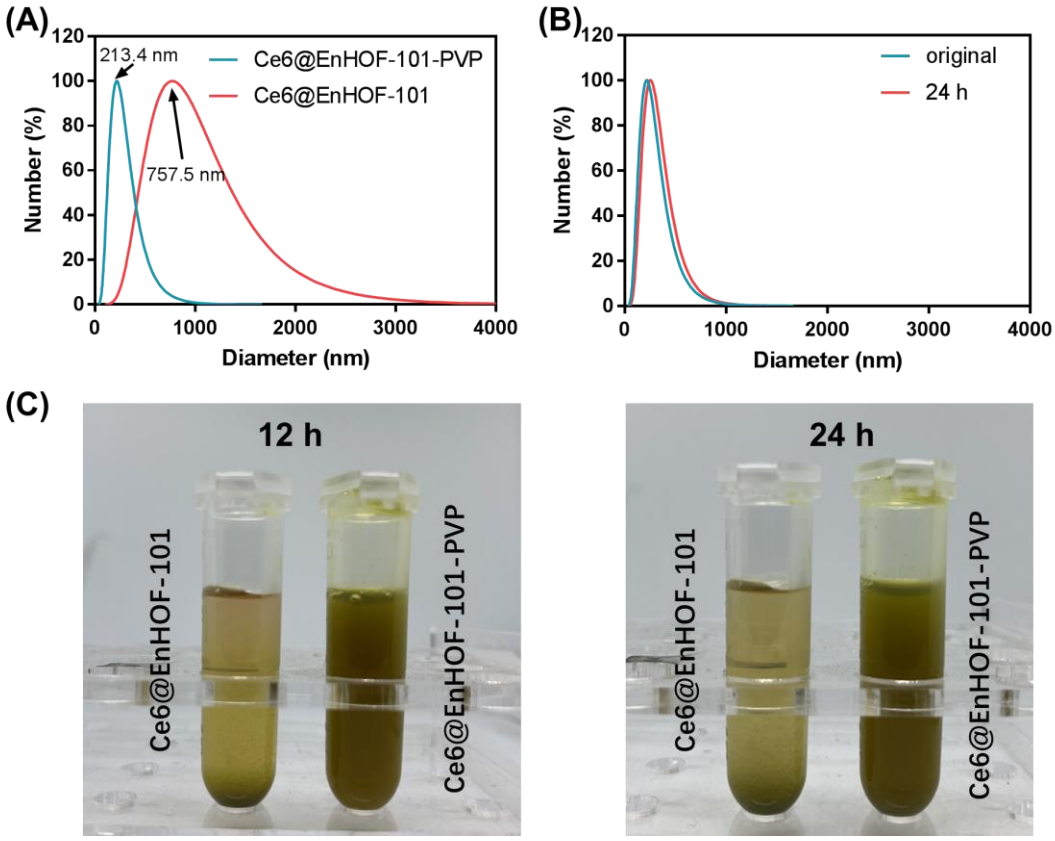

Figure S18. (A) The particle size distribution of the raw Ce6@EnHOF-101 and Ce6@EnHOF-101-PVP. (B) The particle size distribution of Ce6@EnHOF-101-PVP after placing at room temperature for 24 h. (C) The photographs of Ce6@EnHOF-101 and Ce6@EnHOF-101-PVP after standing at room temperature for 12 h and 24 h, respectively. The raw Ce6@EnHOF-101 was coagulated, while the Ce6@EnHOF-101 modified with PVP remained a homogeneous solution.

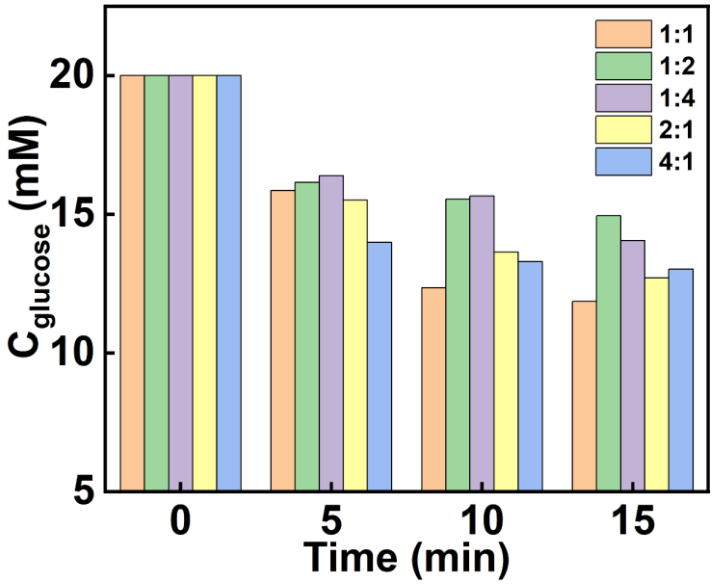

Figure S19. Time-dependent glucose consumption of EnHOF-101 prepared with different ratios of GOx to CAT. The concentrations of all nanoparticles in the trials remained the same (1 mg/mL).

We compared the time-dependent glucose consumption of the synthesized EnHOF with different ratios of GOx to CAT. As shown in Figure S19, when the GOx: CAT ratio was 1: 1, the synthesized EnHOF-101 possessed the highest capacity towards glucose consumption.

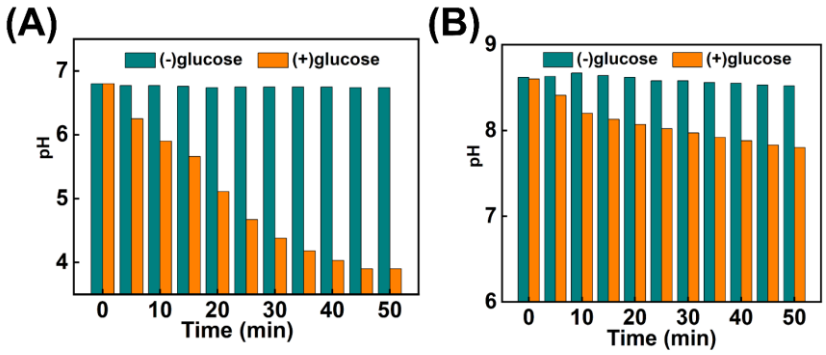

Figure S20. The time-dependent pH value of EnHOF-101 (A) and EnZIF-8 (B) solution in the absence and presence of glucose. Glucose concentration was 20 mM, and the nanoparticles concentration was 1 mg/mL.

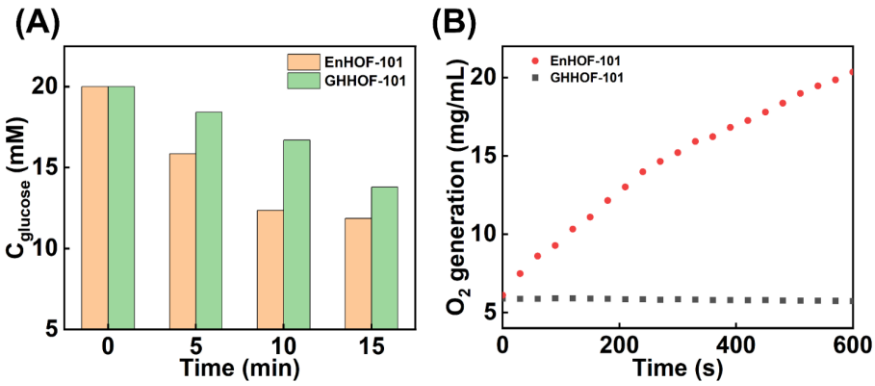

Figure S21. The time-dependent glucose consumption (A) and O_2 generation (B) under the same dosage (1 mg/mL) of EnHOF-101 and GHHOF-101, respectively.

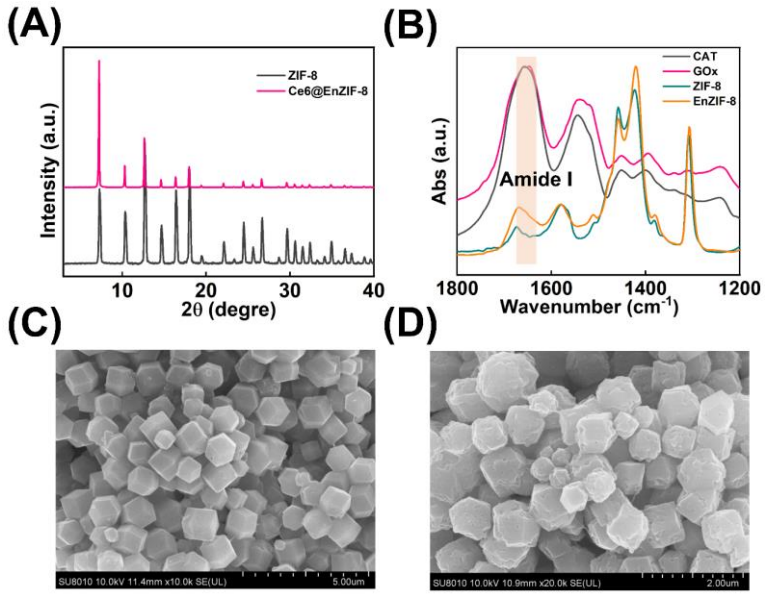

Figure S22. (A) The PXRD patterns. The Ce6@EnZIF-8 inherited the Bragg diffraction pattern of parent ZIF-8, indicating that the framework crystallinity was preserved. (B) The FTIR analysis of EnZIF-8. The spectral band (amide I, 1700−1610 cm^{-1}) in EnZIF-8 was designated as the emblematic peptide skeleton of the enzyme, attesting the successful encapsulation of enzymes. The SEM images of ZIF-8 (C) and EnZIF-8 (D), respectively.

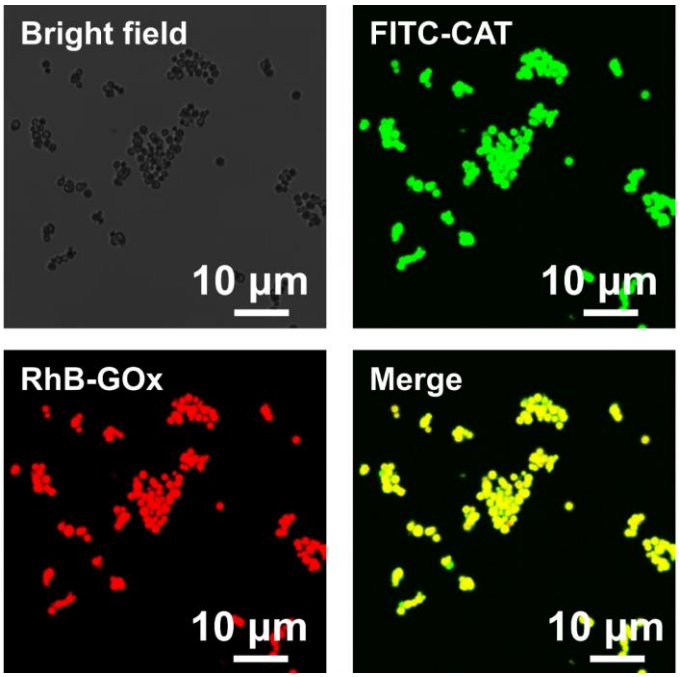

Figure S23. The CLSM images of ZIF-8 after the encapsulation of FITC-CAT and RhB-GOx. The overlapped fluorescence suggested that the FITC-CAT and RhB-GOx were uniformly distributed within a ZIF-8 crystal. This also demonstrated the successful encapsulation of GOx and CAT into ZIF-8.

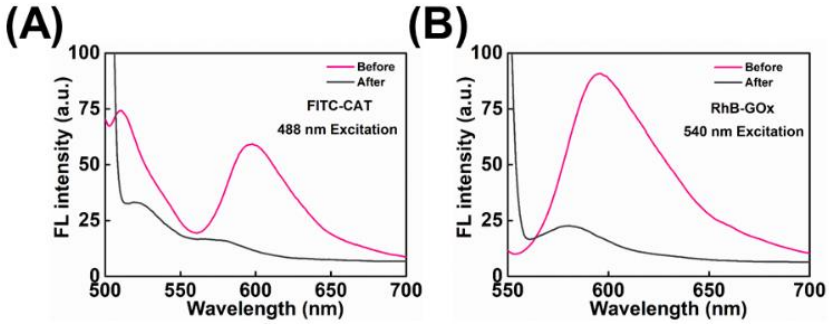

Figure S24. The fluorescence spectra of FITC-CAT (A) and RhB-GOx (B) in the supernatants before and after encapsulation by ZIF-8.

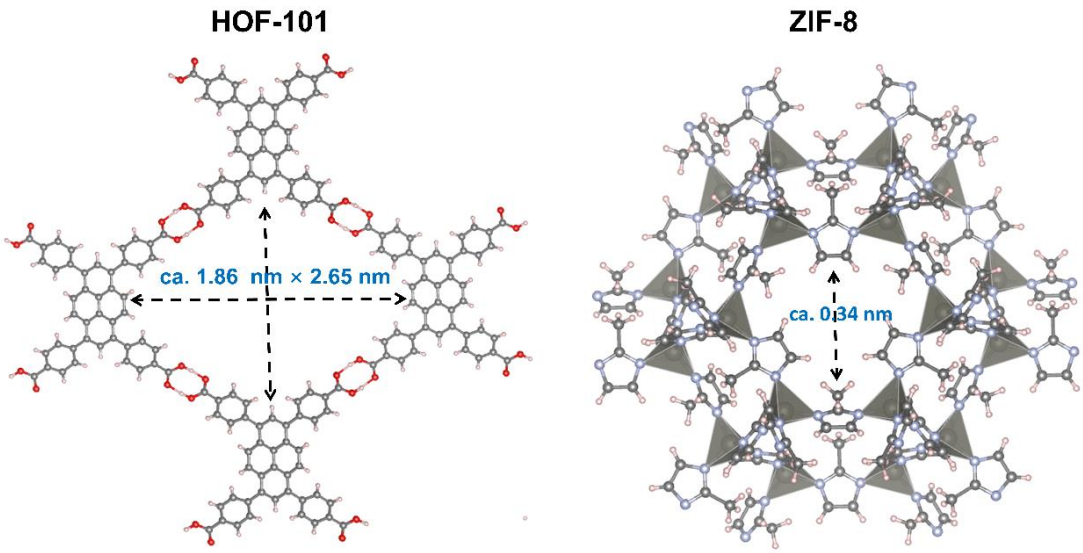

Figure S25. The crystallographic pore structures of HOF-101 and ZIF-8.

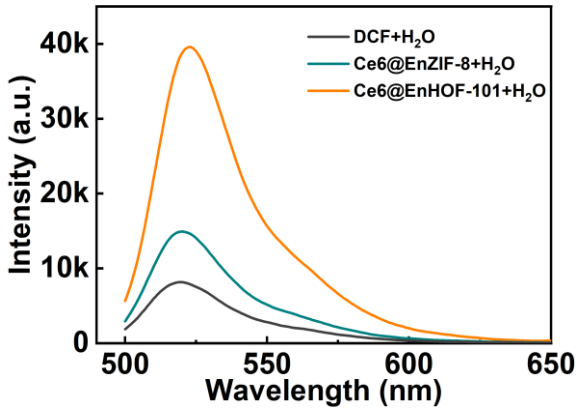

Figure S26. The ROS measurements by fluorescence spectroscopy using DCFH-DA as the probe. The sample was irradiated by white light (45 mW/cm^2) for 10 min before the test.

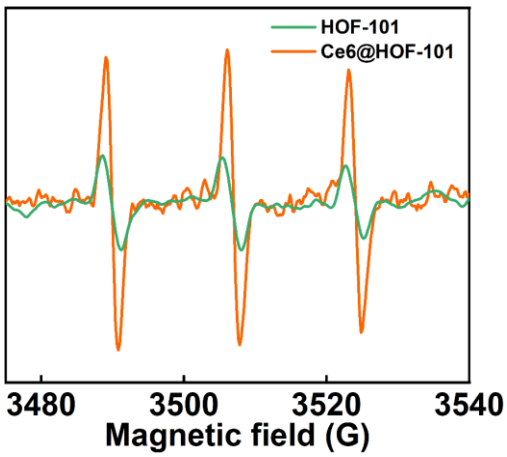

Figure S27. Comparison of the $^1O_2$ generation by EPR in HOF-101 and Ce6@HOF-101 samples. TEMP was used as the $^1O_2$ probe. In addition, the concentrations of all nanoparticles remained the same (1 mg/mL), and all of the trials were irradiated by 45 mW/cm^2 for 10 min before the EPR measurement.

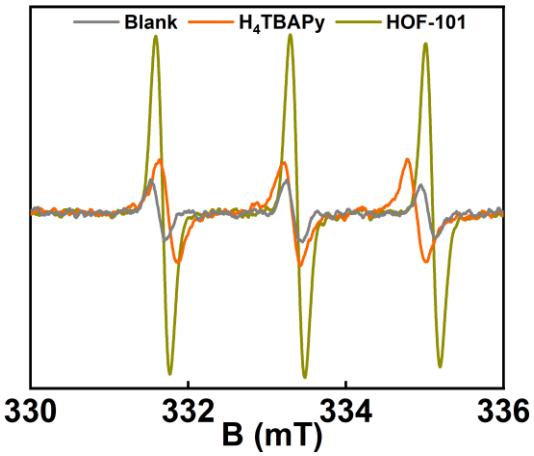

Figure S28. Comparison of the $^1O_2$ generation by EPR in free H4TBAPy (dissolved in DMF) and HOF-101 sample. TEMP was used as the $^1O_2$ probe. In addition, the concentrations of all materials remained the same (1 mg/mL) and all of the trials were irradiated by 45 mW/cm^2 for 10 min before the EPR measurement.

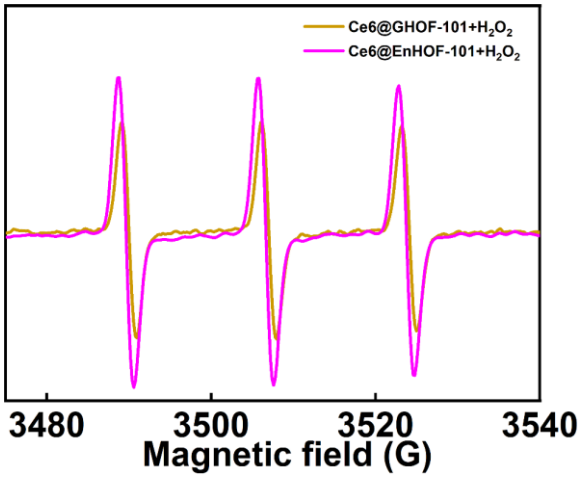

Figure S29. Comparison of the $^1O_2$ generation in the Ce6@GHOF-101 and Ce6@EnHOF-101 samples in the presentence of 20 mM H_2O_2 by EPR. TEMP was used as the $^1O_2$ probe. In addition, the concentrations of all materials remained the same (1 mg/mL), and all of the trials were irradiated by 45 mW/cm^2 for 10 min before the EPR measurement.

The $^1O_2$ generation ability of Ce6@EnHOF-101 was improved in contrast to GHOF-101 under the same H_2O_2 concentration (Figure S29). This was attributed to the continuous supply of O_2 through the H_2O_2 decomposition by CAT (Figure 2C), which in turn facilitated the conversion of O_2 to $^1O_2$ under photocatalysis

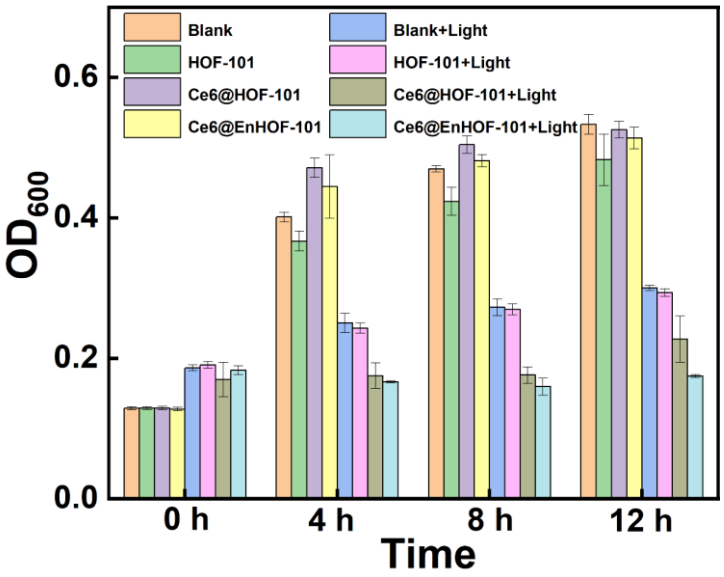

Figure S30. Time-dependent bacterial growth of *MRSA* after treated with different conditions.

The time-dependent bacterial growth has been characterized in Figure S30. It was observed that our Ce6@EnHOF-101 nanoreactor completely inhibited the bacterial growth, while the bacterial growths at different levels were observed in other groups at the same condition. These data further demonstrated the advantages of the photo-bio-catalytic cascade HOFs nanoreactors for diabetic wound therapy.

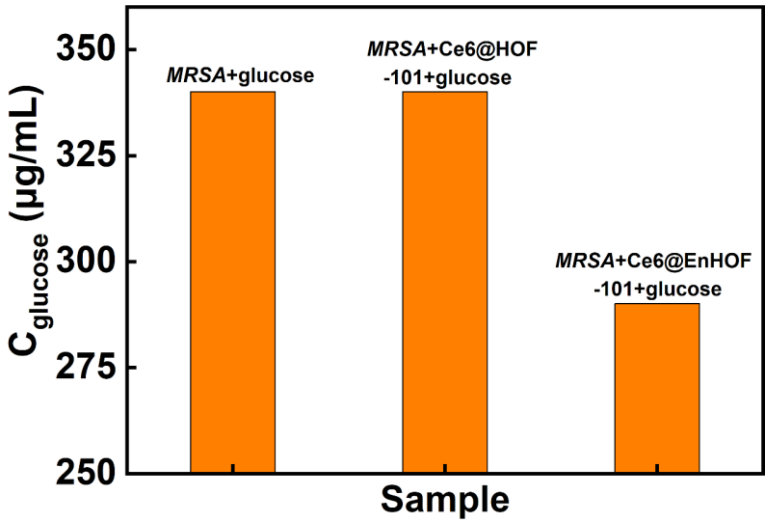

Figure S31. The glucose consumption around the bacterial colony after incubated with different nanomaterials for 12 h.

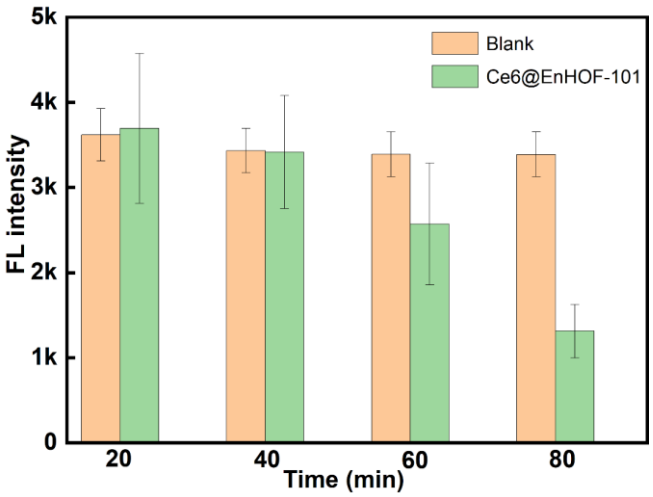

Figure S32. The oxygen levels after incubating the 293T cells with Ce6@EnHOF-101 in the simulated hyperglycemic (20 mM) and H_2O_2-overexpressed (20 μM) microenvironment.

The O_2 was monitored by a fluorescence probe, R01 (Bolsen Biotechnology Co., LTD., shanghai, China). In the fluorescence sensing process, the fluorescence of the probe at 603 nm can be selectively quenched by O_2 molecules. Figure S32 described the time-dependent changes of fluorescence intensity at 603 nm (excitation wavelength: 468 nm) when the 293T cells were incubated with Ce6@EnHOF-101 under the simulated hyperglycemic (20 mM) and H_2O_2-overexpressed (20 μM) microenvironment. The dynamically decreasing fluorescence was recorded under the treatment by Ce6@EnHOF-101 in the dark. It verified that our Ce6@EnHOF-101 indeed could promote the O_2 generation under the simulated hyperglycemic (20 mM) and H_2O_2-overexpressed (20 μM) microenvironment.

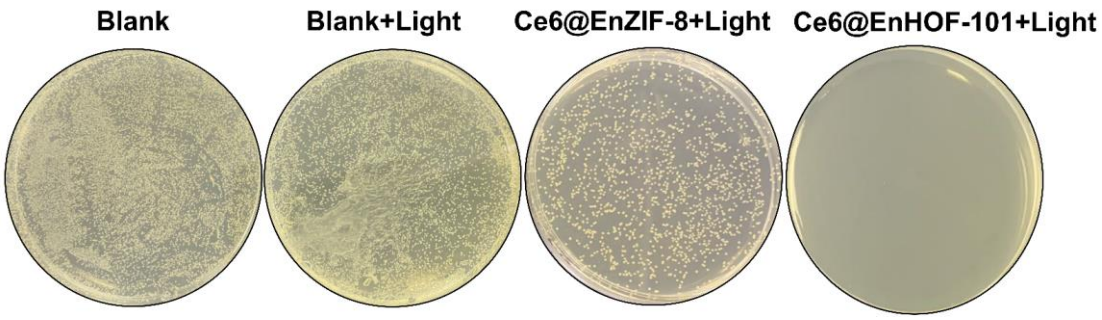

Figure S33. The photographs of bacterial colonies formed by *MRSA* after treatment in different groups. It showed that the antibacterial ability of Ce6@EnHOF-101 was much higher than that of Ce6@EnZIF-8 under similar photodynamic therapy.

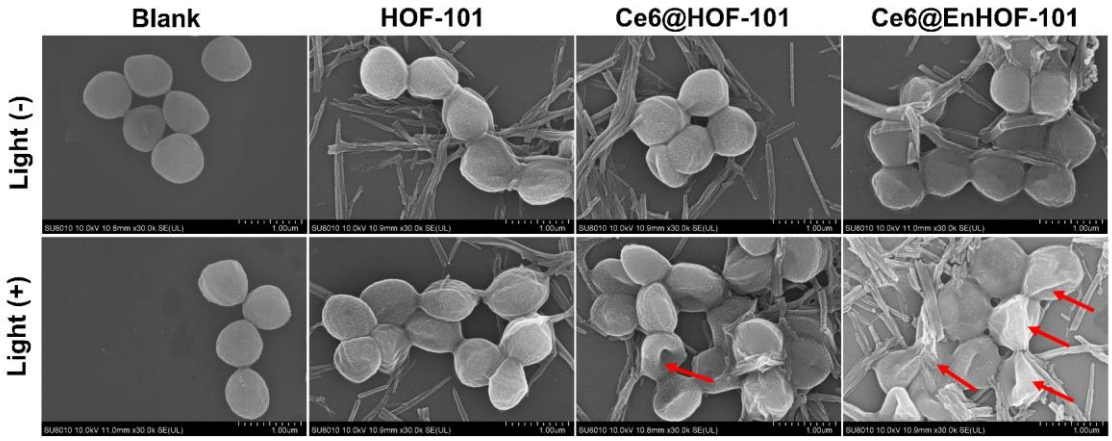

Figure S34. SEM images of the *MRSA* after different treatments. Under white light irradiation, Ce6@HOF-101 led to the partial collapse and shrinkage in the cell membrane. It should be noted that the bacterial membranes were seriously damaged with cell wall fragmentation and completely lost their primary spherical morphologies using our Ce6@EnHOF-101 under similar white light irradiation.

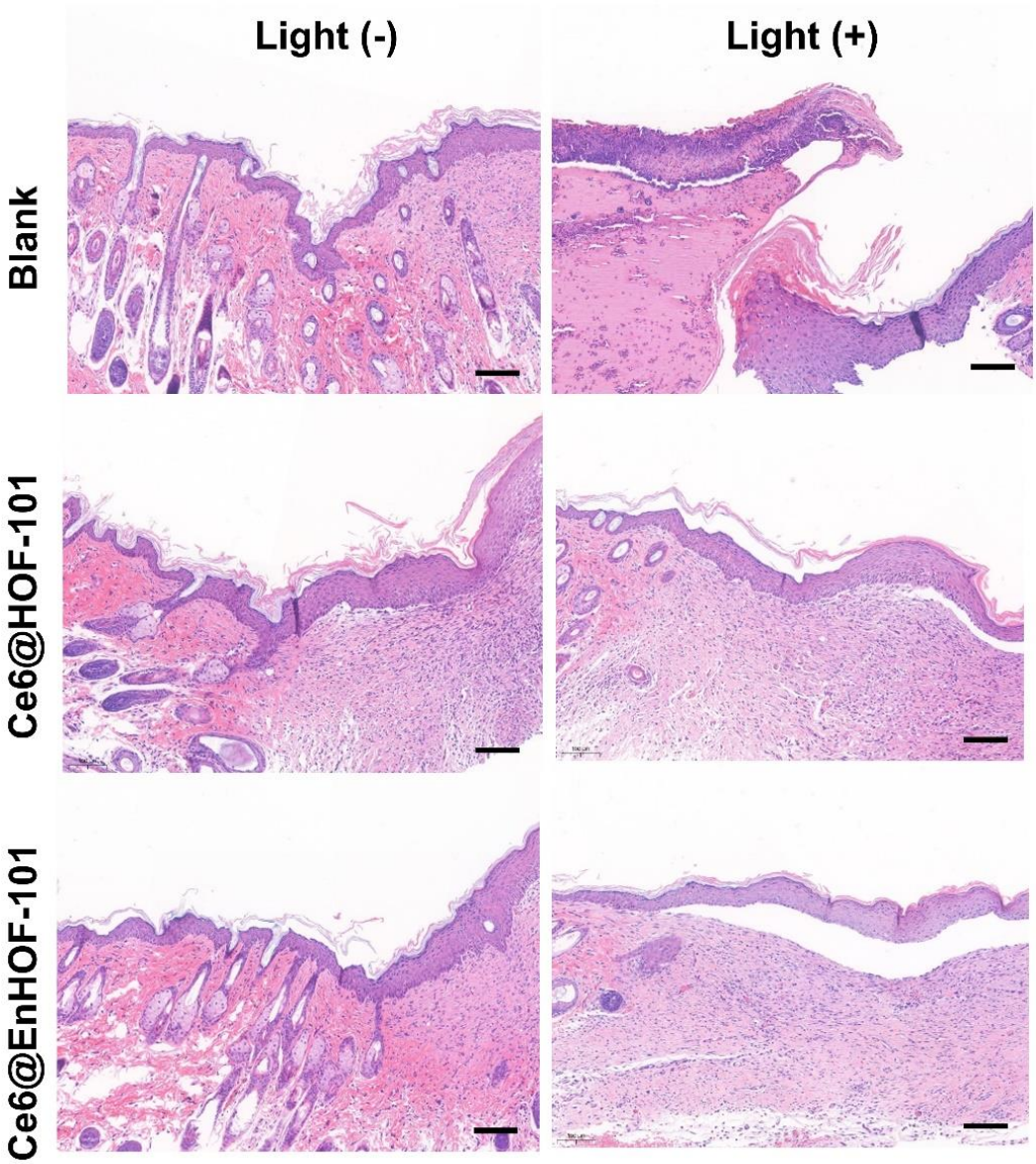

Figure S35. H&E staining images of wound tissue slices after treatment for 12 days by different groups. Scale bar: 100 μm. The data of Ce6@HOF-101 and Ce6@EnHOF-101 under light irradiation were also displayed in Figure 4D in main text. There were many incomplete epidermal layers for the groups of blank, bank+light, Ce6@HOF-101, Ce6@HOF-101+light and Ce6@EnHOF-101. It indicated low antibacterial efficiency. Nevertheless, an intact epidermal structure on the wounds was observed in the group of Ce6@EnHOF-101+light. These results demonstrated that our Ce6@EnHOF-101 nanoreactor exhibited better in vivo wound-healing performance under irradiation.

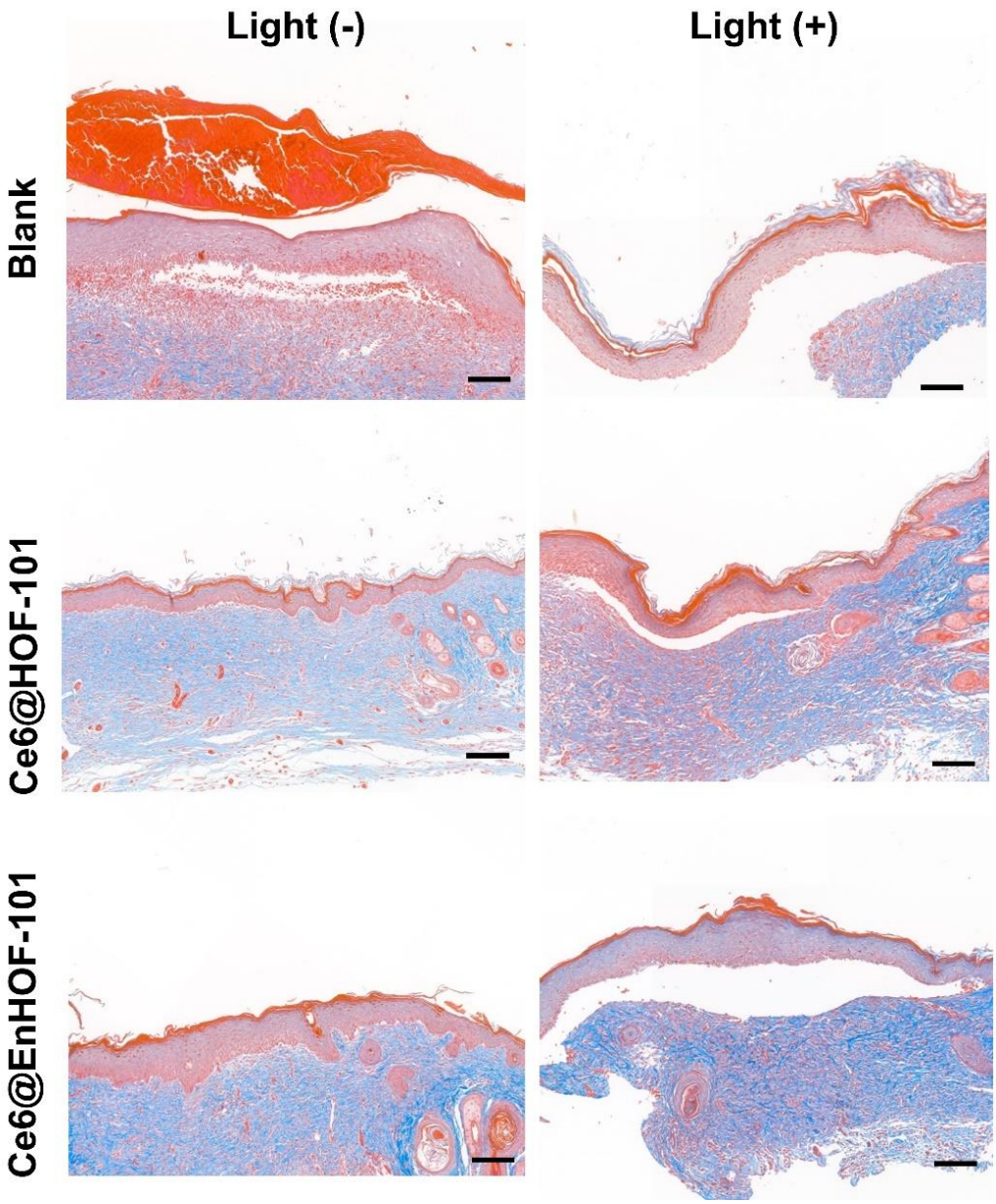

Figure S36. Masson staining images of the wound tissue slices after treatment for 12 days by different groups. Scale bar: 100 μm. The data of Ce6@HOF-101 and Ce6@EnHOF-101 under light irradiation were also displayed in Figure 4D in main text. The maximum collagen fibers were observed in the group of Ce6@EnHOF-101+light, indicating the Ce6@EnHOF-101 could effectively facilitate the healing of infected wounds in vivo under irradiation.

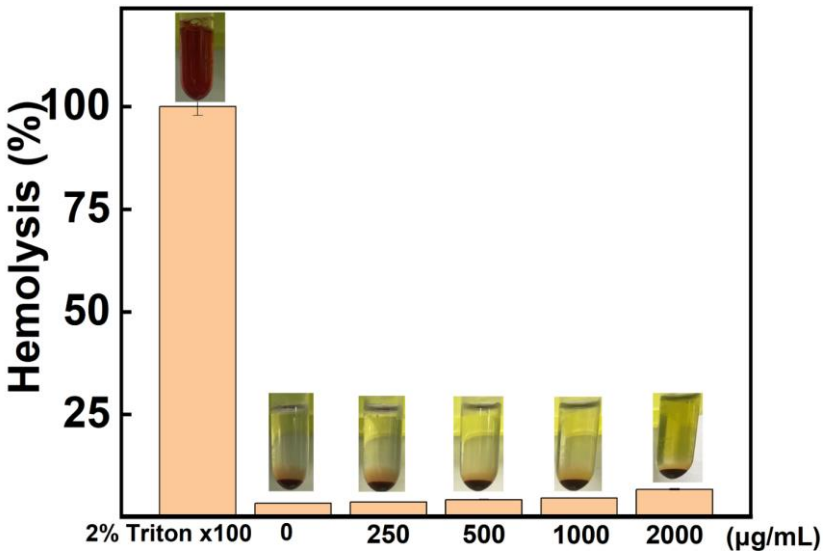

Figure S37. Hemolysis percentage of red blood cell (RBC) (4%, v/v) at various concentrations of Ce6@EnHOF-101. No obvious hemolysis was observed when a series of concentrations of Ce6@EnHOF-101 were co-cultured with RBC.

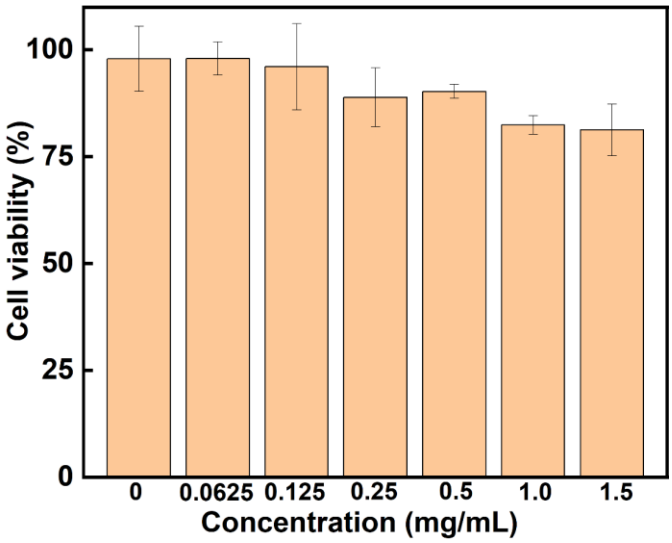

Figure S38. The relative cell viability of 293T normal cells treated with different concentrations of Ce6@EnHOF-101 for 12 h.

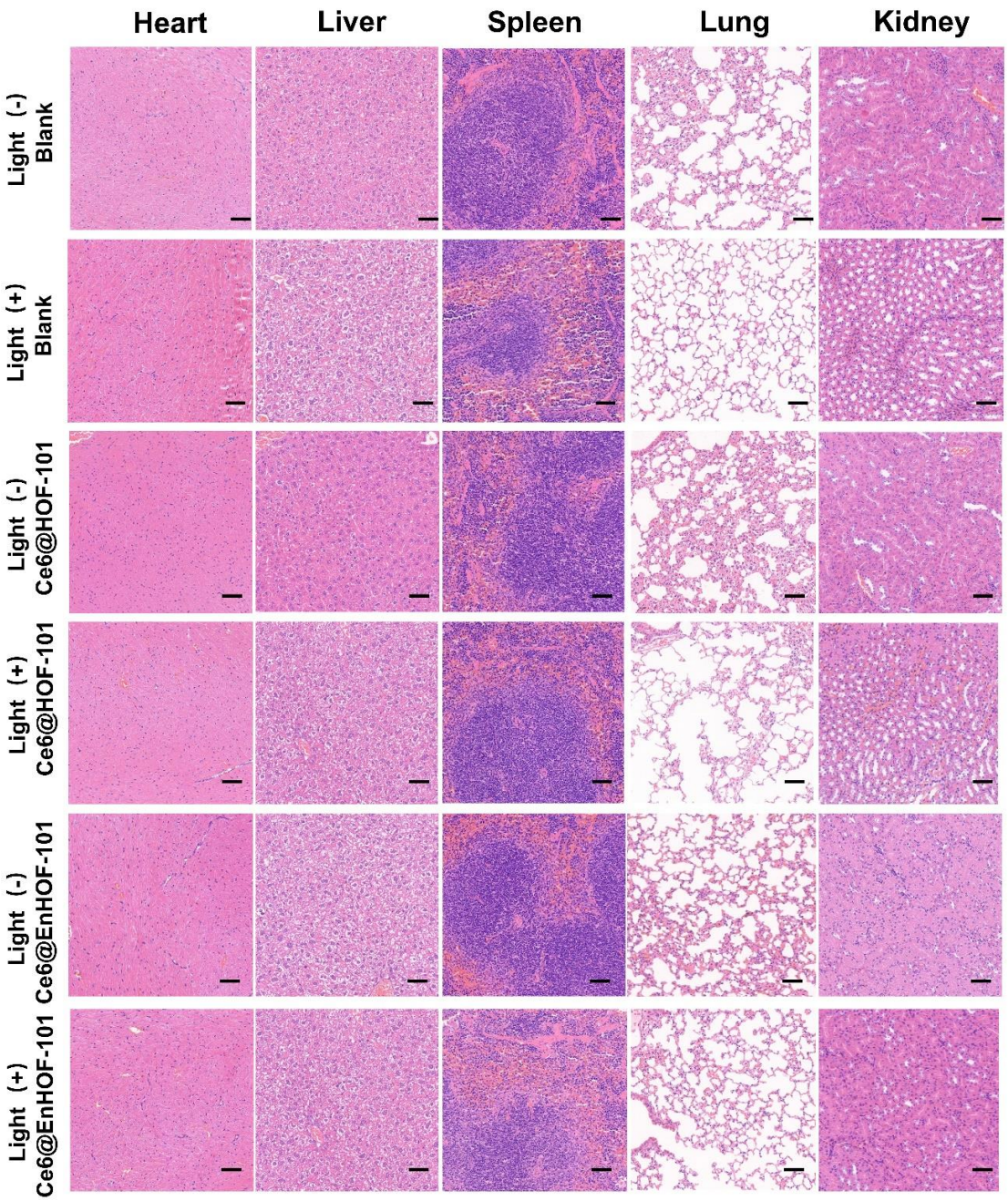

Figure S39. Histological images of the main organs. Scale bar: 50 μm. There was no obvious inflammation or lesions in the main organs after the photodynamic therapy by Ce6@EnHOF-101, which revealed the good biocompatibility of Ce6@EnHOF-101 nanoreactor.

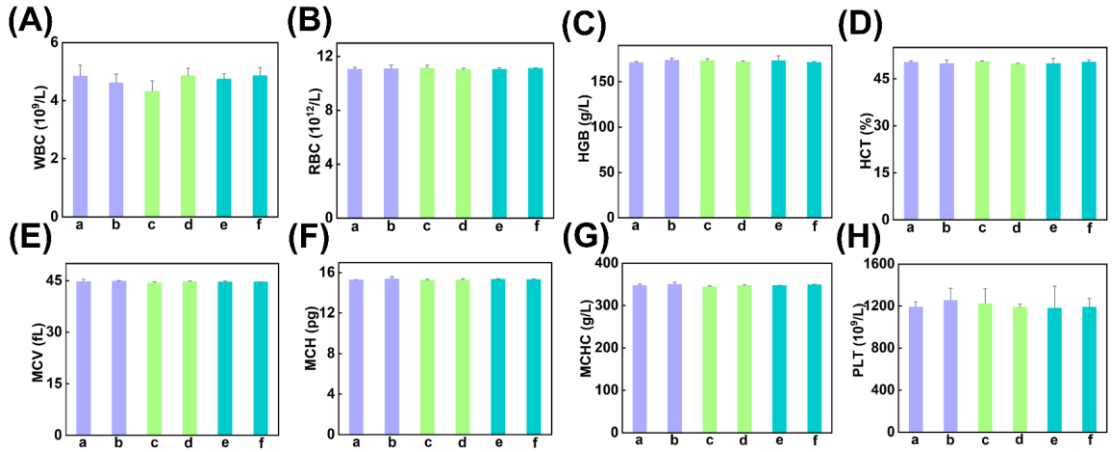

Figure S40. The routine blood test of the mice. The detected indicators included: (A) white blood cells (WBC), (B) red blood cells (RBC), (C) hemoglobin (HGB), (D) hematocrit (HCT), (E) mean corpuscular volume (MCV), (F) mean corpuscular hemoglobin (MCH), (G) mean corpuscular hemoglobin concentration (MCHC) and (H) platelets (PLT). The letters from a to f in each Figures represent the different testing groups: a) blank, b) blank+light, c) Ce6@HOF-101, d) Ce6@HOF-101+light, e) Ce6@EnHOF-101, and f) Ce6@EnHOF-101+light, respectively.

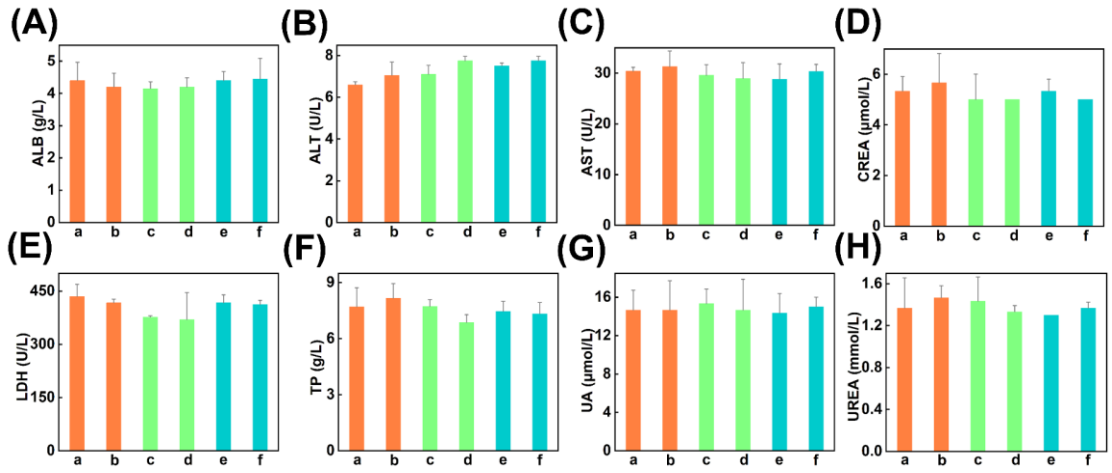

Figure S41. The blood biochemical analyses of the mice. The testing indicators include: (A) albumin (ALB), (B) alanine aminotransferase (ALT), (C) aspartate aminotransferase (AST), (D) creatinine (CREA), (E) lactate dehydrogenase (LDH), (F) total protein (TP), (G) uric acid (UA) and (H) urea (UREA). The letters from a to f in each Figures represent the different testing groups: a) blank, b) blank+light, c) Ce6@HOF-101, d) Ce6@HOF-101+light, e) Ce6@EnHOF-101, and f) Ce6@EnHOF-101+light, respectively.

Supplementary References

(1) Chen, G.; Huang, S.; Shen, Y.; Kou, X.; Ma, X.; Huang, S.; Tong, Q.; Ma, K.; Chen, W.; Wang, P.; Shen, J.; Zhu, F.; Ouyang, G. Protein-Directed, Hydrogen-Bonded Biohybrid Framework. *Chem* **2021**, *7*, 2722-2742.

(2) Chen, G.; Huang, S.; Kou, X.; Zhu, F.; Ouyang, G. Embedding Functional Biomacromolecules within Peptide-Directed Metal-Organic Framework (MOF) Nanoarchitectures Enables Activity Enhancement. *Angew. Chem. Int. Ed*. **2020**, *59*, 13947-13954.

(3) Liao, F.-S.; Lo, W.-S.; Hsu, Y.-S.; Wu, C.-C.; Wang, S.-C.; Shieh, F.-K. Morabito, J. V.; Chou, L.-Y.; Wu, K. C. W.; Tsung, C.-K. Shielding against Unfolding by Embedding Enzymes in Metal-Organic Frameworks via a de Novo Approach. *J. Am. Chem. Soc.* **2017**, *139*, 6530-6533.

(4) Yin, Q.; Zhao, P.; Sa, R.-J.; Chen, G.-C.; Lü, J.; Liu, T.-F.; Cao, R. An Ultra-Robust and Crystalline Redeemable Hydrogen-Bonded Organic Framework for Synergistic Chemo-Photodynamic Therapy. *Angew. Chem. Int. Ed.* **2018**, *57*, 7691-7696.

(5) Bradford, M. M. A Rapid and Sensitive Method for the Quantitation of Microgram Quantities of Protein Utilizing the Principle of Protein-dye Binding. *Anal. Biochem.* **1976**, *72*, 248-254.

(6) Bourré, L.; Thibaut, S.; Briffaud, A.; Rousset, N.; Eléouet, S.; Lajat, Y.; Patrice, T. Indirect Detection of Photosensitizer Ex Vivo. *J. Photochem. Photobiol. B Biol.* **2002**, *67*, 23-31.

(7) Chen, W.; Ouyang, J.; Yi, X.; Xu, Y.; Niu, C.; Zhang, W.; Wang, L.; Sheng, J.; Deng, L.; Liu, Y.-N.; Guo, S. Black Phosphorus Nanosheets as a Neuroprotective Nanomedicine for Neurodegenerative Disorder Therapy. *Adv. Mater.* **2018**, *30*, 1703458

.